

Comparison of electron-nucleus quasi-elastic cross sections using spectral functions with (e, e') data from 0.5 GeV to 1.5 GeV and effects on neutrino quasi-elastic cross sections

Hiroki Nakamura ^{a *}, Ryoichi Seki ^{b, c †}, Makoto Sakuda ^{d ‡ §}

^aDepartment of Physics, Waseda University, Tokyo 169-8555, Japan

^bDepartment of Physics,
California State University, Northridge, California 91330, USA

^cW.K. Kellogg Radiation Laboratory, 106-38,
California Institute of Technology, Pasadena, California 91125, USA

^dInstitute for Particles and Nuclear Studies, KEK, Tsukuba, 305-0801, Japan

We carry out a relativistic calculation of the cross sections of electron-¹⁶O and -¹²C quasi-elastic scattering and quasi-free Δ production and compare with the (e, e') data systematically in the wide energy range of 0.5 – 1.5 GeV. Using the same formalism, we examine the ν_μ quasi-elastic scattering from ¹⁶O. The model incorporating the nuclear correlation effects agrees better with the electron-nucleus scattering data than a uniform Fermi-Gas model. In the neutrino quasi-elastic scattering, the nuclear correlation has an appreciable effect on the cross section of high-energy scattered leptons, and it may have an important consequence in the neutrino oscillation measurements aiming at a few % precision.

1. Introduction

The field of neutrino physics is developing rapidly after atmospheric neutrino oscillations and solar neutrino oscillations have been established [1,2,3]. Recently, SK collaboration has found an evidence for the oscillatory signature in atmospheric neutrinos, improving the determination of Δm^2 [4], and K2K experiment has confirmed the neutrino oscillations of atmospheric neutrinos at the 99.99% CL [5,6]. These neutrino experiments measure the energy and angle of muons produced in neutrino-nucleus interactions and obtain the incident neutrino energy that determines the neutrino oscillations. K2K takes data at $E_\nu=0.5-3$ GeV region, and the recent L/E analysis of the SK atmospheric neutrinos is based on the dataset mainly from 0.5 to 25 GeV. JPARC

and NuMI neutrino experiments [7,8] propose to measure $\nu_\mu \rightarrow \nu_e$ oscillations and to determine Δm^2 at 1% level of the precision and $\sin^2 2\theta_{13}$ above 0.006, using a narrow-band neutrino beam at $E_\nu = 0.8$ GeV (JPARC) and 2.0 GeV (NuMI, off-axis).

It is thus vital that theoretical calculations of the cross sections and spectra could be carried out with a similar reliability. For this, both of neutrino-nucleus reactions and relevant nuclear structure have to be well under control. At $E_\nu=3$ GeV or less, quasi-elastic scattering and quasi-free Δ production dominates the neutrino-nucleus reactions. The reactions at this energy region are associated with a wide range of the momentum transfer and thus involve various aspects of nuclear structure. Because the momentum transfer involved is large enough that nuclear correlations are important as the relevant nuclear structure beyond a mean-field description. Furthermore, the neutrino-nucleus reactions do occur, in fact rather appreciably, with a small momentum

*naka@hep.phys.waseda.ac.jp

†rseki@krl.caltech.edu

‡sakuda@fphy.hep.okayama-u.ac.jp

§Present address: Department of Physics, Okayama University, Okayama, 700 -8530 Japan

transfer, and requires a careful treatment of nuclear properties and reactions, as observed in the deficit of events in the low $Q^2 < 0.2$ (GeV/c)² region [6,9], compared to what is expected based on a Fermi gas model.

In this paper, we focus on the aspects of effects of nuclear correlations. Using the same formalism, we study both of electron and neutrino quasi-elastic scattering in the energy range of 0.5 and 1.5 GeV. For numerical calculations, we mostly take ¹⁶O as it is the main target nucleus in SK, K2K, and other experiments. We calculate the cross sections of electron-¹⁶O quasi-elastic scattering and quasi-free Δ production, using a relativistic plane-wave-impulse approximation (PWIA) formalism [10,11] with a uniform Fermi-gas model and a spectral function [12], and compare with (e, e') data, so as to examine the validity of the calculation. The PWIA neglects final-state interactions, but we will estimate their effects using simple formalisms. Following the electron scattering, we examine neutrino-¹⁶O scattering to see how the effects observed in the electron scattering manifest in the neutrino scattering.

2. Formalism

Electron-nucleus quasi-elastic cross section is expressed as

$$\frac{d\sigma}{dE'd\Omega} = \frac{k'}{8(2\pi)^4 M_A E} \int d^3\mathbf{p} F(\mathbf{p}, \mathbf{q}, \omega) \sum_{\text{spin}} |\mathcal{M}_{eN}|^2, \quad (1)$$

where E is the incident electron energy, M_A the mass of the target nucleus, E' and k' the energy and momentum of the scattered electron, respectively. \mathcal{M}_{eN} is the invariant amplitude of electron-nucleon elastic scattering. $F(\mathbf{p}, \mathbf{q}, \omega)$ is the nuclear effect contribution expressed in terms of \mathbf{p} , \mathbf{q} and ω ; the initial nucleon momentum, the momentum transfer, and the energy transfer, respectively. $F(\mathbf{p}, \mathbf{q}, \omega)$ is proportional to the imaginary part of the $1p1h$ Green's function. For high-energy scattering, we apply a factorization approximation, a convolution of the $1p$ and $1h$ Green's functions:

$$F(\mathbf{p}, \mathbf{q}, \omega) =$$

$$\frac{1}{2M_A} \int d\omega' P_h(\mathbf{p}, \omega') P_p(\mathbf{p} + \mathbf{q}, \omega - \omega'). \quad (2)$$

Here, $P_h(\mathbf{p}, \omega)$ is proportional to the $1h$ Green's function, and is proportional to the nuclear spectral function. The spectral function describes the probability of removing a nucleon of the momentum \mathbf{p} with the removal energy ω from the nucleus, which is usually referred to as the (nuclear) spectral function. $P_p(\mathbf{p}, \omega)$ is proportional to the $1h$ Green's function. It describes the probability for adding a nucleon, thus describing the final-state interactions of the knocked-out nucleon as it goes out the residual target nucleus.

For the neutrino-nucleus quasi-elastic cross section, the invariant amplitude of electron-nucleon scattering is replaced by that of neutrino-nucleon scattering [13] with the same $F(\mathbf{p}, \mathbf{q}, \omega)$. For the quasi-free Δ production cross section, different forms are used for both of the invariant amplitude and $P_p(\mathbf{p}, \omega)$.

The electron-nucleon scattering amplitudes used in this calculation are of the standard form, but we use the most up-to-date vector nucleon form factors [14,15] and $N - \Delta$ transition form factors [16]. As to the invariant neutrino-nucleon amplitude, we use the standard dipole form factor with $M_A = 1.07$ GeV.

The models used in this paper are the relativistic, simple Fermi-gas model (FG) and a realistic spectral function model (SF). FG was used by E. Moniz and his collaborators more than three decades ago [17,18]. It is known to yield a good description of the total cross section, but to fail to provide a reliable detailed description such the transverse and longitudinal cross sections separately [19]. In FG, $P_h(\mathbf{p}, \omega)$ and $P_p(\mathbf{p}, \omega)$ are given by

$$P_h(\mathbf{p}, \omega) = \frac{1}{E_p} \theta(P_F - |\mathbf{p}|) \delta(E_p + \omega) \quad (3)$$

$$P_p(\mathbf{p}', \omega) = \frac{1}{E'_p} \theta(|\mathbf{p}'| - P_F) \delta(E'_p - \omega), \quad (4)$$

where E_p is the effective Fermi-momentum parameter, $E_p = \sqrt{p^2 + M^2} - E_B$ with E_B the effective nuclear binding-energy parameter and M the nucleon mass, and $E'_p = \sqrt{p'^2 + M^2}$. In our calculation, we take P_F to be 225 MeV and E_B

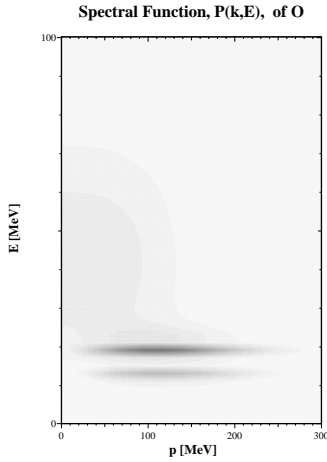


Figure 1. Contour plot of spectral function $P(\mathbf{p}, E)$ of ^{16}O [20].

27 MeV [18]. Note that Eq. (4) describes the Pauli blocking condition in the final state.

SF uses a more realistic description of the initial, ground-state nucleus. $P_h(\mathbf{p}, \omega)$ and $P_p(\mathbf{p}, \omega)$ in this model are given by:

$$P_h(\mathbf{p}, \omega) = \frac{1}{E_p} P(\mathbf{p}, \omega) \quad (5)$$

$$P_p(\mathbf{p}', \omega) = \frac{1}{E'_p} \delta(E'_p - \omega), \quad (6)$$

where $P(\mathbf{p}, \omega)$ is the spectral function. In this work, we use $P(\mathbf{p}, \omega)$ that was calculated by Benhar *et al.* [20], which includes the nuclear shell structure combined with the short-range correlations under a local density approximation. Note that Eq. (6) for $P_p(\mathbf{p}, \omega)$ represents the PWIA we use.

3. Numerical results

3.1. e-nucleus quasi-elastic scattering and quasi-free Δ production

We now compare our calculation with electron- ^{16}O scattering data at various incident energies.

For a reference, we also include the results for electron- ^{12}C quasi-elastic scattering. The experimental data we compare to are $^{16}\text{O}(e', e)$ at the scattering angle $\theta = 32^\circ$ for the incident energy $E = 0.7, 0.88, 1.08, \text{ and } 1.2$ GeV [21], $^{12}\text{C}(e', e)$ at $\theta = 60^\circ$ for $E = 0.5$ GeV [22] and at $\theta = 50.4^\circ$ for $E = 0.78$ GeV [23].

Figure 2 includes four figures of the ^{16}O cross sections at the four incident energies. The quasi-elastic scattering contribution appears as the most prominent peak on the left-handed side of each figure. We see that FG overestimates the quasi-elastic contribution at all energies, but SF agrees with the data better especially above 1 GeV. The FG quasi-elastic contribution has a parabola shape, but the SF contribution has tails at both sides of the energy, especially prominent on the high energy side. In SF, the strength at the peak is reduced, moving mostly to the high-energy tail region, as a consequence of the inclusion of high-momentum components due to nuclear correlations, in the spectral function in $F(\mathbf{p}, \mathbf{q}, \omega)$. FG and SF yield similar contributions to the quasi-free Δ peak, in a good agreement with the data at all energies. In the “dip” region between the two peaks, both of the FG and SF contributions are smaller than the data. SF gives, however, larger contributions than FG and thus a better agreement with the data, again as a consequence of the inclusion of nuclear correlations in $F(\mathbf{p}, \mathbf{q}, \omega)$.

In Fig. 3 we show a similar calculation for electron- ^{12}C quasi-elastic scattering. We see the same trend here.

We also examined the final-state interaction effects using a simple model based on high-energy nucleon-nucleus optical potential [24]. In this, $P_p(\mathbf{p}, \omega)$ of SF is changed as:

$$\begin{aligned} P_p(\mathbf{p}', \omega) &= \frac{1}{E'_p} \delta(E'_p - \omega) \\ &\rightarrow \frac{1}{E'_p} \frac{W/\pi}{(\omega - E'_p)^2 + W^2/4}, \end{aligned} \quad (7)$$

where the imaginary part of the potential W is related to the mean-free path of the outgoing nucleon and is written as

$$W = \frac{1}{2} v \rho \sigma_{NN} \quad (8)$$

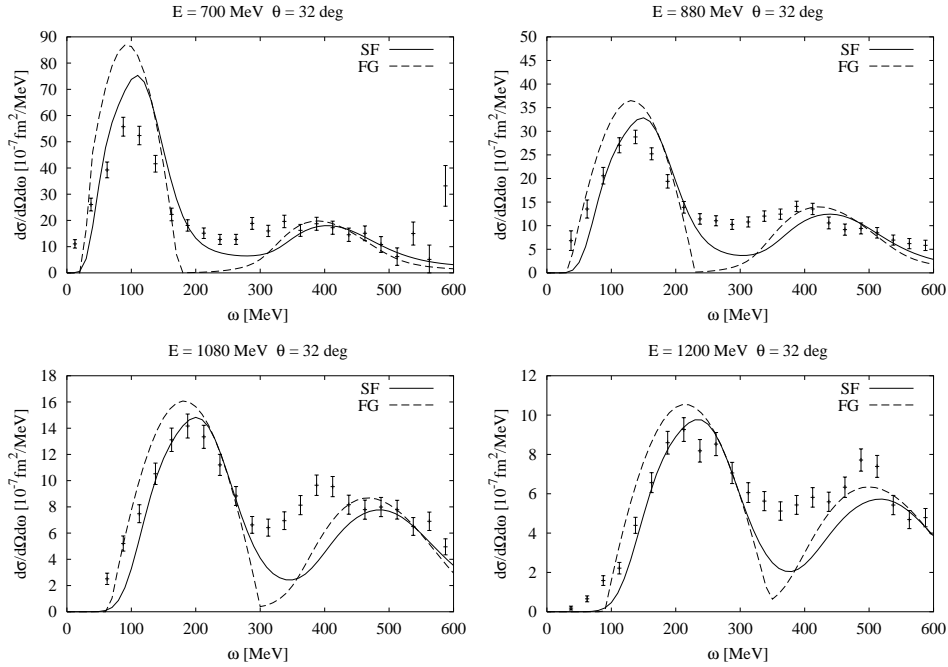


Figure 2. Combined cross sections of electron- ^{16}O quasi-elastic scattering and quasi-free Δ resonance production, using a spectral function (SF, solid curves) and a simple Fermi gas model (FG, dash curves), compared with the (e, e') data [21].

in terms of the nucleon density ρ and the nucleon-nucleon cross section σ_{NN} . We use $\rho = 0.16 \text{ fm}^{-3}$ and $\sigma_{NN} = 40 \text{ mb}$ for this simple estimate. Figure 4 shows that the final-state interactions move the strength in the quasi-elastic peak to the tail regions, and thus broaden the quasi-elastic peak. We see that the deficit in the strength between the two peaks of the quasi-elastic scattering and quasi-free Δ production is somewhat reduced and the agreement with the data is improved somewhat.

In this work, we have not considered other pion production process than the quasi-free Δ production. For this, some phenomenological [25] and theoretical work [26] are available. We leave this issue and others, such as exchange-current contributions, as future work.

3.2. ν_{μ} - ^{16}O quasi-elastic scattering

We now turn to the ν_{μ} - ^{16}O quasi-elastic scattering.

First, we examine the momentum-transfer Q^2 dependence of the differential cross section using FG and SF. Near the forward, Q^2 is small and the Pauli blocking (PB) plays the major role even in this high-energy region. Accordingly, in addition to the use of the same FG as before, we use two-types of SF; without PB as previously shown in Eq. (6), and with PB as

$$\begin{aligned}
 P_p(\mathbf{p}', \omega) &= \frac{1}{E'_p} \delta(E'_p - \omega) \\
 &\rightarrow \frac{1}{E'_p} \theta(|p'| - P_F) \delta(E'_p - \omega). \quad (9)
 \end{aligned}$$

In this way, we include in SF a part of final-state interaction effects, which is generated by PB.

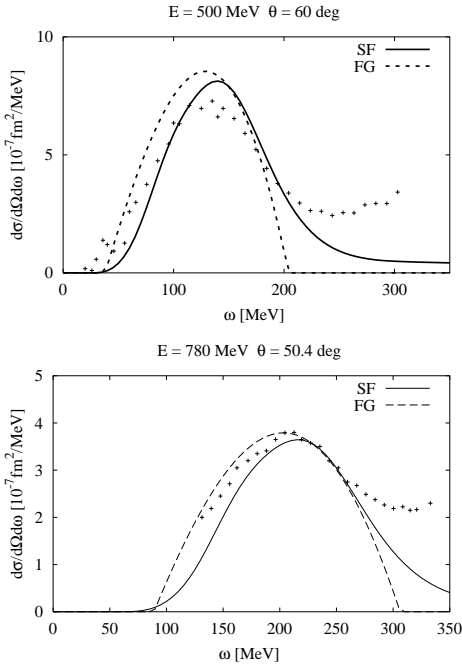


Figure 3. $^{12}\text{C}(e', e)$ quasi-elastic scattering cross section using FG model (dotted curves) and SF model (solid curves), compared with the (e, e') data [21,22].

$P_p(\mathbf{p}', \omega)$ takes a more complicated form when the effects are included more realistically, and the calculation here is a simple estimate.

The ν_μ - ^{16}O quasi-elastic cross section thus calculated is shown in Fig. 5. By comparing the cross sections by the two types of SF cross sections, with and without PB, we see that the Pauli blocking clearly plays a decisive role and that the cross sections calculated by SF with PB and by FG are quite close in the low Q^2 region. This is reasonable since SF with PB and FG use the same $P_p(\mathbf{p}', \omega)$ by incorporating PB in the same way.

Note that the the small Q^2 contribution is usually not considered in the case of electron scattering as the cross section diverges for $Q^2 \rightarrow 0$ and also the incident beam line experimentally

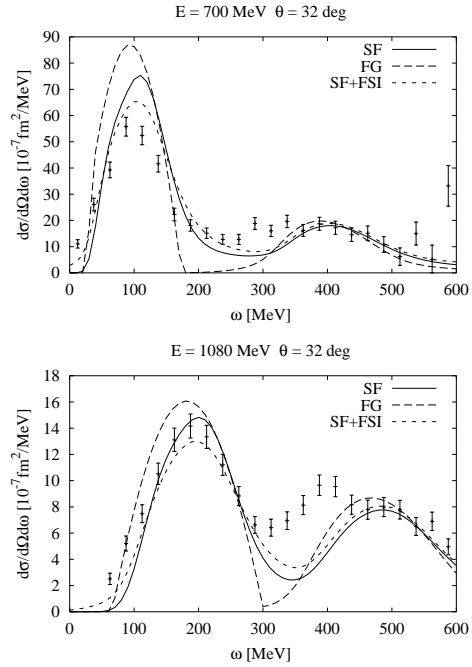


Figure 4. Combined cross section of electron- $^{16}\text{O}(e', e)$ quasi-elastic scattering and quasi-free Δ resonance production. the figure is the same as Fig. 2, except for SF with the final-state interaction is added and is shown using the dotted curves.

prevents a measurement close to forward. In the case of the high-energy neutrino scattering, the situation is quite different as we know: Ample events appear near the forward, making it vital to understand the forward depression as shown in Fig. 5. We note that, though not shown here, the electron scattering cross sections given in Figs. 2-3 are changed little by the inclusion of the Pauli Blocking effect (9). The momentum transfer associated with the kinematics examined in these figures is large.

Second, we examine the ν_μ -nucleus cross sections as a function of the scattered muon energy. Figure 6 compares the cross sections calculated by the three different ways as before: FG and SF

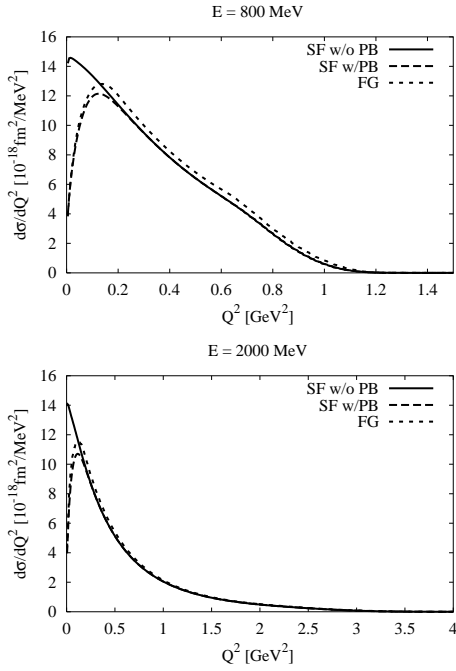


Figure 5. Differential cross section of $^{16}\text{O}(\nu_\mu, \mu^-)$ quasi-elastic scattering as a function of square of the momentum transfer Q^2 at the neutrino incident energy $E = 0.8$ and 2.0 GeV. The cross sections are shown, calculated using SF without and with the Pauli blocking (solid and dash curves, respectively) and FG (dotted curves).

with and without PB. The difference between SF with and without PB observed in low Q^2 region in Fig.5 corresponds to that at the higher end of E_μ spectrum in this figure. FG yields a larger high-energy peak contribution. This difference is *not* due to the Pauli blocking, but due to the nuclear correlation effects in the spectral function: The difference is after all associated with scattered muons at a high energy. This difference should show up in the forward angle cross section. We emphasize that *this difference may have a direct effect on neutrino oscillation measurements.*

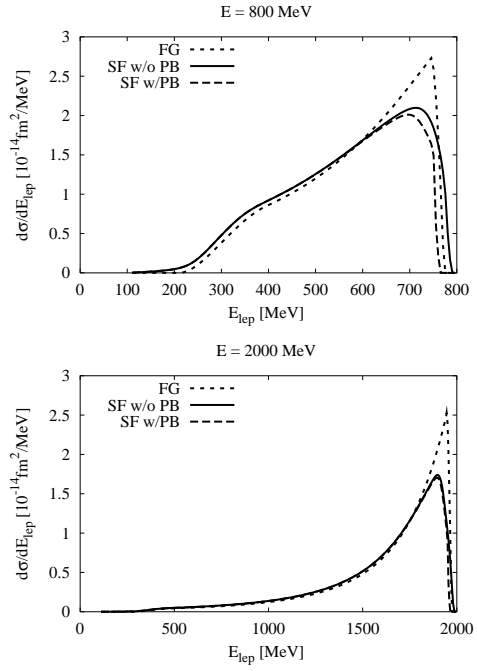


Figure 6. Differential cross section of $^{16}\text{O}(\nu_\mu, \mu^-)$ quasi-elastic scattering as a function of the scattered muon energy for $E = 0.8$ and 2.0 GeV, using SF without and with the Pauli blocking (PB) (solid and dash curves, respectively) and FG (dotted curves).

4. Conclusion

We have carried out a relativistic calculation of the cross sections of electron- ^{16}O and ^{12}C quasi-elastic scattering and quasi-free Δ production and have compared with the data systematically in the wide energy range of $0.5 - 1.5$ GeV. Using the same formalism, we have then examined the ν_μ quasi-elastic scattering from ^{16}O .

We find that Spectral function calculation agrees better with the experimental data $A(e, e')$ than a uniform Fermi-gas model. In particular, this is important to explain the "dip region" between the quasi-elastic interaction and the delta production kinematics. A uniform Fermi-gas

model cannot fill the dip region. In addition, the total cross section does not change between the uniform Fermi-Gas model and the spectral function calculation within 10%, but the differential cross section as functions of the scattered muon energy changes as much as 20–30%. We think that this is very important for the future neutrino experiments aiming at 1% or better precision.

Acknowledgement

We thank Omar Benhar for providing us his spectral functions of ^{12}C and ^{16}O . This work is supported by the Japan Society for the Promotion of Science through the Grant-In-Aid for Scientific Research (15540299), and by the US Department of Energy (DE-FG02-87ER40347) at CSUN and by the US National Science Foundation (NSF0244899) at Caltech.

REFERENCES

1. Y. Fukuda *et al.*(SK collaboration), Phys. Rev. Lett. **81**(1998), 1562.
2. S. Fukuda *et al.*(SK collaboration), Phys. Lett. **B539**(2002), 179. Q. R. Ahmad *et al.*(SNO collaboration), Phys. Rev. Lett. **89**(2002),011301; *ibid*, Phys. Rev. Lett. **89**(2002),011302.
3. K. Eguchi *et al.*(KamLAND collaboration), Phys. Rev. Lett. **90**(2003),021802.
4. Y. Ashie *et al.*(SK collaboration), Phys. Rev. Lett. **93**(2004), 101801.
5. M. H. Ahn *et al.*(K2K), Phys. Rev. Lett. **90**(2003), 041801(2003);
6. T. Nakaya (K2K collaboration), a talk at Neutrino2004, Paris, June 16-19, 2004.
7. Y. Itow *et al.*, The JHF-Kamioka neutrino project, hep-ex/0106019.
8. M. Messier, a talk at Neutrino2004.
9. T. Ishida, Nucl. Phys. (Proc. Suppl.) **112**(2002), 132.
10. R. A. Smith and E. J. Moniz, Nucl. Phys. **B43**(1972), 605.
11. H. Nakamura and R. Seki, Nucl. Phys. (Proc. Suppl.) **112**(2002), 197.
12. O. Benhar *et al.*, Nucl. Phys. **A579**(1994), 493.
13. C.H. Llewellyn Smith, Phys. Rept. **3** (1972) 261.
14. E. J. Brash, A. Kozlov, S. Li and G. M. Huber, Phys. Rev. C **65** (2002) 051001.
15. P. E. Bosted, Phys. Rev. C **51** (1995) 409.
16. E. Paschos, J.-Y. Yu and M. Sakuda, Phys. Rev. D **69**(2004),014013.
17. E. J. Moniz, Phys. Rev. **184** (1969) 1154.
18. E.J. Moniz, I. Sick, R.R. Whitney, J.R. Ficenec, R.D. Kephart and W.P. Trower, Phys. Rev. Lett. **26** (1971) 445.
19. P. Barreau *et al.*, Nucl. Phys. **A402**, 515 (1981); M. Deady *et al.*, Phys. Rev. C **28**, 631 (1983); Z. Meziani *et al.*, Phys. Rev. Lett. **52**, 2130 (1984); R. Altemus *et al.*, Phys. Rev. Lett. **44**, 965 (1980); T. C. Yates *et al.*, Phys. Lett. B **312**, 382 (1993); A. Zghiche *et al.*, Nucl. Phys. **A572**, 513 (1994); J. Jourdan, Phys. Lett. B **353**, 189 (1995), and Nucl. Phys. **A603**, 117 (1996); and A. Fabrocini, Phys. Rev. C **55**, 338 (1997).
20. Private communication from O. Benhar. The method of the calculation is described in: O. Benhar, A. Fabrocini, S. Fantoni, and I. Sick, Nucl. Phys. **A579** (1994) 493; and references therein.
21. M. Anghinolfi *et al.*, Nucl. Phys. **A602** (1996) 405.
22. R. R. Whitney, I. Sick, J. R. Ficenec, R. D. Kephart and W. P. Trower, Phys. Rev. C **9**, 2230 (1974).
23. G. Garino *et al.*, Phys. Rev. C **45** (1992) 780.
24. O. Benhar, A. Fabrocini, S. Fantoni, G. A. Miller, V. R. Pandharipande and I. Sick, Phys. Rev. C **44** (1991) 2328; and O. Benhar, contribution to NuInt02, to appear *Proc. NuInt02*.
25. C. Keppel, *Inclusive nucleon resonance electroproduction at large momentum transfer*, UMI-95-29706 (1994); and Ph.D.Thesis, American Univ. (1995).
26. J. Nieves, J. E. Amaro, and M. Valverde, reported in this workshop, nucl-th/0408008; and a preprint, nucl-th/0408005.